

NAVIDA: Vision-Language Navigation with Inverse Dynamics Augmentation

Weiye Zhu^{1*} Zekai Zhang^{1*} Xiangchen Wang^{1*} Hwei Pan¹
Teng Wang¹ Tiantian Geng¹ Rongtao Xu^{2,3} Feng Zheng^{1,3†}

¹ SUSTech, Shenzhen, China

² MBZUAI, Abu Dhabi, United Arab Emirates

³ SpatialTemporal AI, Shenzhen, China

Abstract. Vision-and-Language Navigation (VLN) requires agents to interpret natural language instructions and act coherently in visually rich environments. However, most existing methods rely on reactive state-action mappings without explicitly action-grounded visual dynamics modeling. Lacking awareness of how actions transform subsequent visual observations, agents cannot plan actions rationally, leading to unstable behaviors, weak generalization, and cumulative error along trajectory. To address these issues, we introduce NAVIDA (**N**avigation with **I**nverse **D**ynamics **A**ugmentation), a lightweight VLN framework that incorporates inverse dynamics supervision (IDS) as an explicit objective to embed action-grounded visual dynamics into policy learning. By jointly optimizing this visual dynamics with instruction-conditioned action prediction in a shared representation and action space, NAVIDA provides additional structured supervision that regularizes learning and leads to more stable and consistent navigation. To structure this supervision and extend the effective planning range, NAVIDA employs hierarchical probabilistic action chunking (HPAC), which organizes trajectories into multi-step chunks and provides discriminative, longer-range visual-change cues. Extensive experiments show that NAVIDA achieves superior navigation performance compared to state-of-the-art methods with fewer parameters (3B vs. 8B). Real-world robot evaluations further validate the practical feasibility and effectiveness of our approach. Code is available at <https://github.com/waynechu1021/NAVIDA>.

Keywords: Vision-and-Language Navigation · Inverse Dynamics

1 Introduction

Vision-and-Language Navigation (VLN) [3,17,31] is a challenging multimodal sequential decision-making task, requiring an agent to navigate effectively through a 3D visual environment based solely on natural language instructions. Accordingly, effective VLN requires not only precise instruction comprehension but

* Equal contribution

† Corresponding author

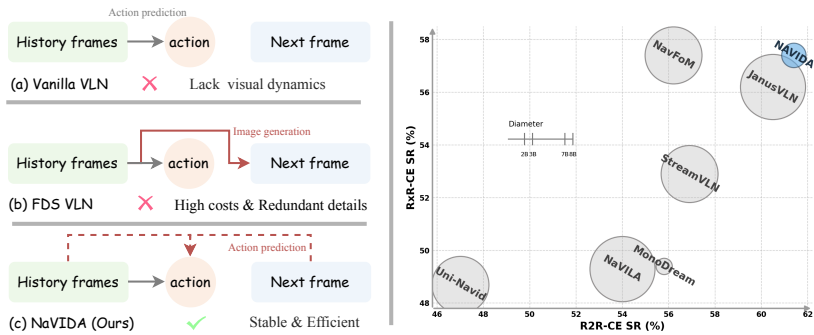


Fig. 1: **Left:** Comparison of three VLN paradigms. (a) Vanilla VLN relies on reactive state-action mapping, lacking the action-grounded visual dynamics; (b) Forward Dynamics Modeling (FDM) adds an additional image generation task which predicts future observations but is compute-heavy and distractible; (c) NAVIDA leverages inverse dynamics supervision to learn action-grounded visual dynamics through action prediction alone, resulting in more efficient and stable training. **Right:** Success rate versus model size comparison. NAVIDA (the blue one) achieves superior performance with smaller model size. The diameter of each circle is proportional to the model size (in billions of parameters).

also long-horizon temporal modeling and robust generalization to visually diverse, unseen scenes. Motivated by advances in video-based Multimodal Large Language Models (MLLMs) [4, 21, 46], recent studies [7, 33, 37, 43, 44, 47] have integrated these models into VLN to exploit their superior visual perception, semantic understanding, and cross-scene generalization.

Many existing works [7, 43, 44] typically formulate VLN as a short-sighted state-to-action strategy. As shown in the left panel of Fig. 1(a), this “Vanilla VLN” paradigm directly maps current language instructions and past visual observations to a limited set of subsequent actions. However, this reactive formulation lacks an explicit notion of action-grounded visual dynamics: *how current visual observations are transferred to the next visual observation through the influence of actions*. Without internalizing these visual dynamics, the agent merely learns shallow correlations between instructions and observations. Consequently, it cannot anticipate the visual consequences of the executed actions, rendering the navigation process highly susceptible to minor perceptual deviations, which inevitably accumulate over long horizons, leading to severe navigational instabilities, such as stopping too early or uncorrectable trajectory drift. To alleviate this issue, recent studies [14, 33, 45] have explored Forward Dynamics Modeling (FDM, as illustrated in Fig. 1b), which forces the agent to predict future visual observations. While FDM explicitly incorporates environmental dynamics into policy learning, it is inherently resource-intensive. Generating high-dimensional future frames often requires complex auxiliary modules (e.g., diffusion-based world models [5, 8]) and introduces significant computational overhead [30, 45]. More critically, FDM suffers from an inherent objective misalignment: recon-

structuring dense, pixel-level future frames forces the model to focus on redundant appearance details (e.g., lighting or textures) that are entirely irrelevant to navigation, rather than on optimizing the structured action space.

Recognizing that effective navigation does not require predicting every future pixel, we propose NAVIDA (left panel of Fig. 1c), a VLN framework that incorporates inverse-dynamics supervision (IDS) as an auxiliary objective to introduce action-grounded visual dynamics into policy training. Rather than relying solely on instruction–action correlations, IDS trains the model to infer actions from visual transitions, encouraging consistency between predicted actions and the observable state changes they induce. This action-grounded supervision provides dense and language-agnostic training signals. By jointly aligning IDS with instruction-based action prediction within a shared feature and action space, NAVIDA facilitates the learning of visual motion representations that capture how actions drive environmental transitions—without requiring dense image prediction or access to future frames. To better structure this supervision and extend the effective planning horizon, we introduce a Hierarchical Probabilistic Action Chunking (HPAC) mechanism that progressively merges low-level actions into multi-level chunks. This hierarchical and stochastic merging strategy compacts short micro-motions into more informative training targets, providing richer and more discriminative signals for inverse dynamics learning. By introducing controlled randomness into chunk boundaries, HPAC avoids overly rigid compression, preserves segmentation diversity, and improves robustness to minor execution variations. As a result, the agent learns to reason over extended temporal spans while maintaining stable and consistent navigation behavior. Extensive experiments demonstrate the effectiveness of NAVIDA by achieving state-of-the-art (SOTA) performance on the VLN-CE [17] benchmark with substantially fewer parameters (as visually summarized in Fig. 1 Right), establishing a simple and lightweight paradigm for VLN research.

In summary, our contributions are threefold:

- We propose NAVIDA, a novel VLN framework that augments policy learning with action-grounded visual dynamics driven by inverse dynamics supervision (IDS). By aligning these two objectives in a shared feature and action space, NAVIDA achieves more stable and consistent navigation.
- We introduce a Hierarchical Probabilistic Action Chunking (HPAC) mechanism to temporally structure the agent’s trajectory into variable-length semantic units. This design improves robustness to minor execution variations, and provides the inverse-dynamics objective with richer visual-transition cues, effectively extending the planning horizon.
- Comprehensive experiments demonstrate that NAVIDA achieves SOTA performance with fewer parameters. Real-world tests confirm feasibility, robustness, and faster, more efficient execution, demonstrating the practical benefits of our joint action-understanding approach in physical environments.

2 Related Work

Vision-and-Language Navigation. VLN tasks require an embodied agent to perceive, reason, and act in response to natural-language instructions. Early studies [6, 13, 20] focused on discrete navigation on connectivity graphs with panoramic RGB-D inputs, achieving strong in-domain results but relying on heavy sensors and pre-scanned viewpoints. Subsequent works [17, 38] have moved toward continuous control and low-level action prediction to better reflect real-world deployment, while several efforts [1, 12, 23, 28, 29, 34] have investigated monocular RGB or RGB-D variants that relax reliance on panoramic sensing. Concurrently, the emergence of MLLMs has spurred monocular-only VLN systems that leverage vision-language backbones for stronger cross-scene transfer and lower hardware cost [7, 37, 43, 44]. Despite these advances, most existing VLN methods remain limited to reactive state-to-action mappings, neglecting explicit modeling of how executed actions relate to subsequent visual transitions. Without such action understanding ability, agents struggle to anticipate short-horizon observation dynamics, often resulting in unstable turning, premature stopping, and compounding errors over long trajectories. In contrast, NAVIDA introduces inverse-dynamics supervision as a state-transition objective within policy learning. By aligning this with instruction-based action prediction in a shared feature and action space, our approach improves execution stability under monocular sensing.

Dynamic Models in Navigation. Reactive state-action modeling directly maps historical visual observations and natural language instructions to the action space, without explicitly modeling the dependency between visual transitions and executed actions. To mitigate this, early works [10, 19, 39] explored using additional pre-training tasks such as path-mask prediction, image prediction, or image completion. However, these were mostly limited to discrete environmental settings and often relied on extended contextual cues or language instructions. More recent methods [14, 33, 45] attempted to combine forward dynamics modeling and decompose the decision task, predicting future images while simultaneously predicting actions to enable modeling of state transitions. Although effective in some settings, forward models typically require additional modules for high-dimensional prediction, increase compute and memory, and can bias learning toward redundant appearance details that are weakly aligned with the decision space. NAVIDA instead adopts inverse dynamics in a continuous environment: from two adjacent images it directly infers the action that caused the transition, sharing the output space with the reactive policy and avoiding extra generators or decoders. This design reduces optimization difficulty in mapping from image space to action space, improves data efficiency, and injects an action-grounded transition prior constraints that strengthens instruction grounding, yielding stable long-horizon navigation.

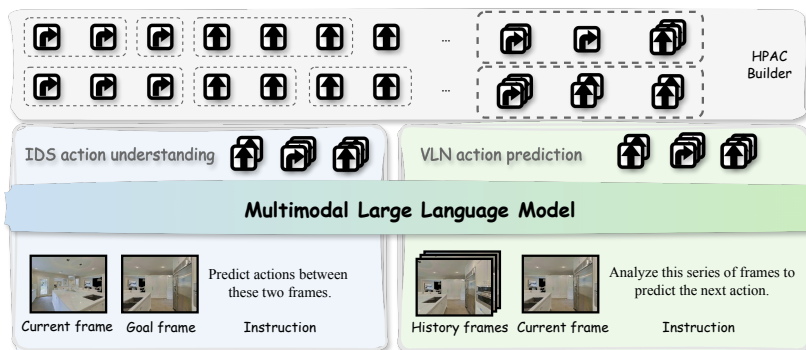


Fig. 2: Overview of NAVIDA. A multimodal language-model backbone generates HPAC action blocks. The HPAC mechanism stochastically merges adjacent actions into variable-length motion units, preserving chunk diversity and improves robustness to minor execution variations. Navigation action prediction and inverse dynamics supervision (IDS) are jointly optimized, enabling action-grounded visual dynamics modeling and strengthens action understanding within a shared representation and action space.

3 NAVIDA Framework

3.1 Preliminary

Task Formulation. The Vision-and-Language Navigation task in continuous environment is defined as follows. At the beginning of each navigation episode, the agent receives a natural language instruction \mathcal{I} . Then, at each time step t , the agent receives an egocentric RGB observation v_t ; we denote the observation history by $\mathcal{V}_{0:t} = \{v_0, \dots, v_t\}$. The discrete action space of the navigation agent is: $\mathcal{A} = \{\text{FORWARD}, \text{TURNLEFT}, \text{TURNRIGHT}, \text{STOP}\}$, and selecting an action $a_t \in \mathcal{A}$ triggers a transition to a new state and yields the next observation v_{t+1} . Episodes terminate when the agent issues STOP or reaches a maximum step budget T_{\max} . When the agent takes a stop action within 3 meters of the target position, the episode is considered successful.

Framework Overview. NAVIDA builds upon a standard Vision–Language Model (VLM) backbone, comprising a visual encoder, a vision–language projector, and an LLM head (Fig. 2). NAVIDA jointly models instruction-based action prediction and action-grounded visual dynamics within a shared feature and action space. To provide structured and discriminative supervision signals, NAVIDA first introduces Hierarchical Probabilistic Action Chunking (HPAC), which organizes temporally adjacent actions into multi-level chunks and captures longer-range visual transition patterns. Built upon this hierarchical structuring, we incorporate inverse-dynamics supervision (IDS) as an auxiliary objective that trains the model to infer actions from visual transitions, strengthening action understanding and visual–action alignment beyond simple instruction–action correlations. Through the joint optimization of action prediction and IDS, NAVIDA achieves more stable and consistent navigation under monocular sensing.

Algorithm 1 Hierarchical Probabilistic Action Chunking

Require: Atomic actions $\mathcal{A} = [a_1, \dots, a_N]$, merge prob. p , max level-2 chunk size n **Ensure:** Hierarchically merged sequence $\mathcal{A}^{(2)}$

```

  {Level-1: Probabilistic merging}
1:  $\mathcal{A}^{(1)} \leftarrow [ ]$ ,  $c \leftarrow [a_1]$ 
2: for  $i = 2$  to  $N$  do
3:   if  $a_i = a_{i-1}$  and  $\text{len}(c) < 3$  and  $\mathcal{U}(0, 1) \leq p$  then
4:     Append  $a_i$  to  $c$ 
5:   else
6:     Append  $c$  to  $\mathcal{A}^{(1)}$ ;  $c \leftarrow [a_i]$ 
7:   end if
8: end for
9: Append  $c$  to  $\mathcal{A}^{(1)}$ 
  {Level-2: Deterministic merging}
10:  $\mathcal{A}^{(2)} \leftarrow [ ]$ ,  $c' \leftarrow [\mathcal{A}_1^{(1)}]$ 
11: for  $i = 2$  to  $|\mathcal{A}^{(1)}|$  do
12:   if  $\text{len}(c') < n$  then
13:     Append  $\mathcal{A}_i^{(1)}$  to  $c'$ 
14:   else
15:     Append  $c'$  to  $\mathcal{A}^{(2)}$ ;  $c' \leftarrow [\mathcal{A}_i^{(1)}]$ 
16:   end if
17: end for
18: Append  $c'$  to  $\mathcal{A}^{(2)}$ 
19: return  $\mathcal{A}^{(2)}$ 

```

3.2 Hierarchical Probabilistic Action Chunking

Instead of predicting a fixed small number of next actions, NAVIDA represents control as variable-length chunks to (a) amplify action-induced visual change for inverse-dynamic supervision and (b) allow farther-ahead decoding when confident, while keeping outputs consistent with the VLN action space. We use an HPAC mechanism to merge atomic actions in two stages. In the first probabilistic merging stage, up to 3 temporally adjacent and visually consistent repetitions of the same atomic action are merged into a sub-chunk with probability p . This stochastic merging strategy compacts micro-motions and mitigates label noise, while avoiding the rigid and potentially over-aggressive compression induced by greedy schemes. By introducing controlled randomness into chunk boundaries, it preserves variability in action segmentation and improves robustness to minor execution fluctuations. In the second, deterministic merging stage, up to n consecutive sub-chunks are merged into a final chunk, yielding a sequence that covers between n and $3n$ atomic actions. The resulting grammar preserves fine-grained short-range decisions while permitting farther-ahead decoding when confidence is high, and it amplifies action-induced appearance and viewpoint changes, thereby producing more discriminative supervision signals. The complete procedure is summarized in Algorithm 1. This chunk representa-

tion is used as the training target, providing a unified label space for IDS and navigation action prediction.

3.3 Inverse-Dynamics Supervision

To enable action-grounded visual dynamics modeling without modifying the architecture, we introduce inverse-dynamics supervision (IDS) at the data level. Given an HPAC-induced pair of frames $(v_t, v_{t+\ell})$, the model is required to predict the token sequence of the intervening variable-length action chunk $\mathbf{y}_t = (y_{t,1}, \dots, y_{t,n_t})$ using the same action grammar as VLN (i.e., action-type and numeric tokens). In this formulation, IDS serves as an explicit action-understanding objective, encouraging the model to interpret visual transitions in terms of structured action representations, while VLN remains an instruction-conditioned action-prediction task. By sharing the same feature and action space, the two objectives complement each other: IDS strengthens grounded action understanding from visual evidence, and VLN leverages this representation for language-guided decision making. Supervision at the level of frame pairs and action chunks aggregates multiple micro-motions, resulting in larger parallax and appearance variations and thus providing a more discriminative learning signal in visually ambiguous settings (e.g., symmetry or transient occlusion). Following StreamVLN [37] and JanusVLN [41], we construct supervision data using Habitat [27] trajectories from R2R [3], RxR [18], ScaleVLN [36], and DAgger [26]. For each trajectory, we apply HPAC to define waypoints, and adjacent waypoints determine non-overlapping subsequences, where the start frame is stored as the current view, the end frame as the goal view, and the intervening action chunk as the supervision label. This process yields approximately 2.4M IDS triplets and an additional ~ 2.8 M chunked VLN samples constructed under the same action grammar.

During training, we jointly optimize the IDS and VLN objectives with shared parameters and task-specific prompts. For IDS, the model predicts \mathbf{y}_t from $(v_t, v_{t+\ell})$ under a task-agnostic prompt \mathcal{I}_{IDS} ,

$$\mathcal{L}_{\text{IDS}}^{\tau} = - \sum_t \sum_{j=1}^{n_t} \log p(y_{t,j}^* | y_{t,<j}^*, \mathcal{I}_{\text{IDS}}, v_t, v_{t+\ell}), \quad (1)$$

while for VLN the model predicts the next chunk from the visual history and instruction,

$$\mathcal{L}_{\text{VLN}}^{\tau} = - \sum_t \sum_{j=1}^{n_t} \log p(y_{t,j}^* | y_{t,<j}^*, \mathcal{I}_{\text{NAV}}, v_{<t}). \quad (2)$$

The combined objective $\mathcal{L} = \sum_{\tau \in D} (\mathcal{L}_{\text{VLN}}^{\tau} + \mathcal{L}_{\text{IDS}}^{\tau})$ regularizes the shared representation by encouraging consistency between action-grounded visual dynamics and instruction-conditioned action prediction. Actions inferred from observed transitions are aligned with actions decoded under language guidance, preserving the original VLN action space while avoiding the need to predict high-dimensional future visual appearance.

Table 1: Comparison with state-of-the-art methods on VLN-CE R2R Val-Unseen split. Observations used include panoramic view (Pano.), odometry (Odo.), depth sensor (Depth) and single RGB camera (S.RGB). All results are from their respective papers. *indicates methods using the waypoint predictor. Best results are highlighted in bold, and the second results are underlined.

Method	Venue	VLM # Params	Observation				R2R Val-Unseen			
			Pano.	Odo.	Depth	S.RGB	NE↓	OS↑	SR↑	SPL↑
HPN+DN* [15]	ICCV2021	-	✓	✓	✓		6.31	40.0	36.0	34.0
CMA* [12]	CVPR2022	-	✓	✓	✓		6.20	52.0	41.0	36.0
VLN⊙BERT* [12]	CVPR2022	-	✓	✓	✓		5.74	53.0	44.0	39.0
Sim2Sim* [16]	ECCV2022	-	✓	✓	✓		6.07	52.0	43.0	36.0
GridMM* [34]	ICCV2023	-	✓	✓	✓		5.11	61.0	49.0	41.0
ETPNav* [2]	TPAMI2024	-	✓	✓	✓		4.71	65.0	57.0	49.0
ScaleVLN* [36]	ICCV2023	-	✓	✓	✓		4.80	-	55.0	51.0
InstructNav [22]	CoRL2024	-	-	-	-	-	6.89	-	31.0	24.0
LAW [25]	EMNLP2021	-		✓	✓	✓	6.83	44.0	35.0	31.0
CM2 [11]	CVPR2022	-		✓	✓	✓	7.02	41.5	34.3	27.6
ETPNav + FF [35]	CoRL2024	-		✓	✓	✓	5.95	55.8	44.9	30.4
Seq2Seq [17]	ECCV2020	-			✓	✓	7.77	37.0	25.0	22.0
NavMorph [40]	ICCV2025	-			✓	✓	5.75	56.9	47.9	33.2
NaVid [44]	RSS2024	7B				✓	5.47	49.1	37.4	35.9
NaVILA [7]	RSS2025	8B				✓	5.22	62.5	54.0	49.0
Uni-NaVid [43]	RSS2025	7B				✓	5.58	53.3	47.0	42.7
Aux-Think [32]	NeurIPS2025	8B				✓	6.08	60.0	54.8	46.9
StreamVLN [37]	ICRA2026	7B				✓	4.98	64.2	56.9	51.9
MonoDream [33]	AAAI2026	2B				✓	5.45	61.5	55.8	49.1
InternVLA-N1(S2) [9]	-	7B				✓	4.89	60.6	55.4	52.1
InternVLA-N1(S1+S2) [9]	-	8B			✓	✓	4.83	63.3	58.2	54.0
NavFoM [42]	ICLR2026	7B				✓	5.01	64.9	56.2	51.2
JanusVLN [41]	ICLR2026	8B				✓	<u>4.78</u>	<u>65.2</u>	<u>60.5</u>	56.8
NAVIDA (ours)	-	3B				✓	4.32	69.5	61.4	<u>54.7</u>

4 Experiment

4.1 Experiments Setup

Implementation Details. We implement NAVIDA on top of Qwen2.5-VL-3B [4]. During training, the vision encoder is frozen, while the projector and LLM backbone are optimized with a learning rate of $2e - 5$ for one epoch over mixed VLN and inverse-dynamics data. Following NaVILA [7], we cap the temporal context at eight historical frames; if a sequence exceeds this limit, we uniformly subsample it to eight frames to preserve coverage across the full trajectory. Unless otherwise stated, HPAC uses merge probability $p = 0.7$ and a maximum level-2 chunk size of $n = 3$. At inference, we only execute the first two predicted action chunks. Further hyperparameter details are provided in the Supplementary Material.

Evaluation Benchmarks. We evaluate NAVIDA on VLN-CE using the val-unseen splits of R2R-CE [3, 17] and RxR-CE [17, 18]. Following standard practice [9, 32, 41], we report Navigation Error (NE), Success Rate (SR), Oracle Success rate (OS), Success weighted by Path Length (SPL) and normalized Dynamic Time Warping (nDTW). These metrics jointly capture goal completion,

Table 2: Comparison with state-of-the-art methods on VLN-CE RxR Val-Unseen split. Observations used include panoramic view (Pano.), odometry (Odo.), depth sensor (Depth) and single RGB camera (S.RGB). All results are from their respective papers. Best results are highlighted in bold, and the second results are underlined.

Method	Venue	VLM # Params	Observation				RxR Val-Unseen			
			Pano.	Odo.	Depth	S.RGB	NE↓	SR↑	SPL↑	nDTW↑
NaVILA [7]	RSS2025	8B				✓	6.77	49.3	44.0	58.8
Uni-NaVid [43]	RSS2025	7B				✓	6.24	48.7	40.9	-
Aux-Think [32]	NeurIPS2025	8B				✓	6.24	52.2	40.2	-
StreamVLN [37]	ICRA2026	7B				✓	6.22	52.9	46.0	61.9
MonoDream [33]	AAAI2026	2B				✓	6.38	49.4	40.9	-
InternVLA-N1(S2) [9]	-	7B				✓	6.41	49.5	41.8	62.6
InternVLA-N1(S1+S2) [9]	-	8B		✓		✓	5.91	53.5	46.1	<u>65.3</u>
NavFoM [42]	ICLR2026	7B				✓	<u>5.51</u>	57.4	<u>49.4</u>	60.2
JanusVLN [41]	ICLR2026	8B				✓	6.06	<u>56.2</u>	47.5	62.1
NAVIDA (ours)	-	3B				✓	5.23	57.4	49.6	67.0

trajectory efficiency, and path fidelity, and allow direct comparison to recent RGB-only and multi-sensor approaches. Detailed explanations of the metrics are provided in the Supplementary Material.

Real-World Evaluation Setup. In real-world experiments, we employ two humanoid robot platforms, the AgiBot X2 and the Unitree G1, in an indoor working environment. The AgiBot X2 is equipped with two monocular fisheye RGB cameras; we used only one of them and converted it into an image equivalent to that captured by a pinhole camera. For the Unitree G1, its built-in camera is downward-mounted, and its 55.2° field of view (FOV) cannot cover the area directly in front of the robot. Therefore, we additionally mounted a RealSense D455f camera on its chest. When the robot receives a command, it uploads the current RGB image to NAVIDA deployed on a remote server equipped with an NVIDIA 4090 GPU. NAVIDA outputs the action sequence in 0.93 seconds. After receiving the action command from the server, the robot executes the command through the robot’s motion API.

4.2 Main Results

Performance Evaluation. As shown in Tab. 1 (R2R-CE) and Tab. 2 (RxR-CE), NAVIDA achieves state-of-the-art results on the val-unseen splits using only a single RGB stream and a 3B VLM backbone. On R2R-CE, NAVIDA attains the best NE/OS/SR and the second-best SPL, surpassing the strongest 8B baseline JanusVLN [41] by -0.46 NE, +4.3 OS, and +0.9 SR. On RxR-CE, NAVIDA matches the best SR (57.4) and achieves the best NE/SPL/nDTW, improving over StreamVLN and JanusVLN by +1.2 to +4.5 SR, +2.1 to +3.6 SPL, and -0.83 to -0.99 NE. The consistent gains on the longer and linguistically richer RxR-CE benchmark indicate stronger long-horizon alignment and reduced drift, enabled by IDS and hierarchical chunking. Compared with multi-sensor methods such as ETPNav and NavMorph, NAVIDA’s single-RGB policy remains competitive or superior on core metrics. It also achieves the best perfor-

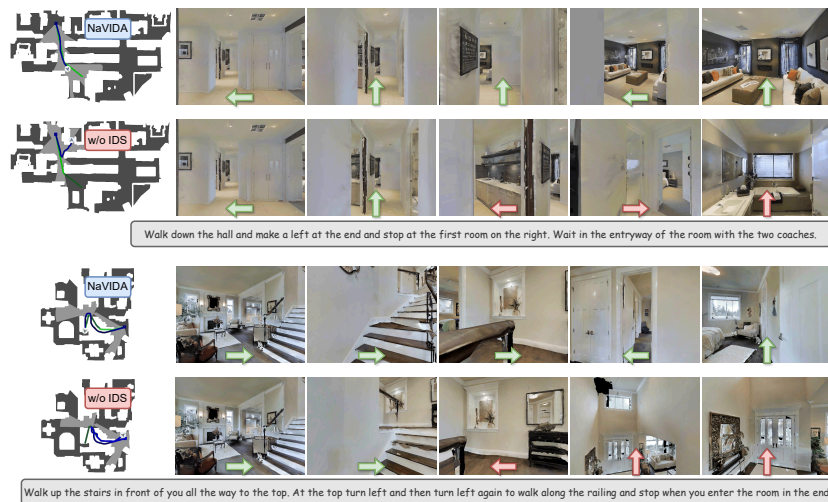


Fig. 3: Qualitative results of NAVIDA on VLN-CE R2R Val-Unseen split. Correct actions are marked with **green arrows**, while incorrect actions are marked with **red arrows**.

Table 3: Ablation study of IDS Data on VLN-CE R2R Val-Unseen split.

R2R	RxR	Dagger	NE↓	OS↑	SR↑	SPL↑
○			7.86	44.5	32.0	27.6
●			6.99	51.5	40.5	35.5
●	●		5.72	57.4	47.7	41.5
●	●	○	5.25	60.9	53.7	47.0
○	○	○	5.29	61.9	52.6	47.1
●	●	●	4.91	63.2	55.5	49.6

Table 4: Ablation study of the IDS Design Variants on VLN-CE R2R Val-Unseen split.

Formulation	NE↓	OS↑	SR↑	SPL↑
w/o IDS	5.29	61.9	52.6	47.1
MCQ	5.82	56.2	49.8	45.7
Noised IDS	6.21	53.9	46.8	42.7
PD	5.27	60.1	52.3	47.8
Ours	4.91	63.2	55.5	49.6

mance among RGB-only methods with only 35% of the parameters and without auxiliary generators or spatial encoders. Overall, these results demonstrate that inverse-dynamics augmentation with HPAC provides an effective and lightweight alternative to conventional map or forward world modeling.

Qualitative Results. Fig. 3 contrasts NAVIDA with a variant without IDS where green arrows mark correct actions and red arrows mark errors. NAVIDA correctly defers turning until clearing the staircase and selects the intended intersection, whereas the ablated model exhibits premature turns and junction misclassification. These are typical symptoms of error accumulation when the model lacks the understanding of action-grounded visual dynamics and fails to internalize the visual consequences of its actions.

Fig. 4 presents examples of real-world trials. NAVIDA executes tight turns at narrow corners and passes smoothly through single-person doorways; even with pedestrians ahead, it resists interference and holds a reliable heading. Taken

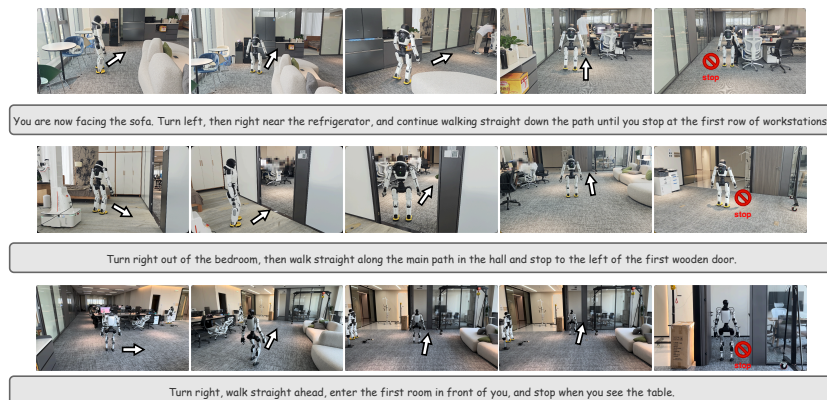


Fig. 4: Real world results of NAVIDA. The robot’s direction of motion is indicated by arrows in the diagram.

together, the simulator and real-world evidence identify IDS as the key component behind the observed stability and scene generalization, outperforming the variant without inverse-dynamics supervision.

4.3 Ablation Study

In this section, we conduct ablations on the effectiveness of IDS, the effectiveness of HPAC and dynamic modeling methods. To ensure efficiency, we conduct experiments on data without ScaleVLN and report the performance on R2R-CE benchmark. Here for convenience, we execute all predicted action chunks in this section.

Scalability of IDS Data. Tab. 3 varies whether R2R, RxR, and DAgger trajectories contribute IDS pairs (●) or not (○). Incorporating IDS consistently improves performance across all metrics and data configurations. On R2R alone, adding IDS increases SR from 32.0 to 40.5. When extending to R2R+RxR, SR further rises to 47.7. Introducing DAgger without IDS yields an SR of 52.6, while enabling IDS supervision across all three sources achieves 55.5 SR, accompanied by a lower NE (4.91) and higher SPL (49.6). Notably, the gains are most pronounced in data-scarce settings and continue to accumulate as additional trajectory sources are introduced. This scaling behavior indicates that IDS provides a complementary training signal rather than merely amplifying imitation supervision. Overall, these results suggest that IDS injects a transferable, language-agnostic notion of action-grounded visual dynamics into the model. Crucially, this capability integrates seamlessly with existing rollout-based paradigms such as DAgger, yielding additive improvements without requiring changes to the underlying imitation framework.

Ablations of IDS Design. To better understand how IDS facilitates action prediction, we conduct ablations on its construction strategy (Tab. 4). First, we corrupt IDS by replacing ground-truth actions with random ones during data

Table 5: Ablation study of HPAC on VLN-CE R2R Val-Unseen split.

Chunk size	Strategy	NE↓	OS↑	SR↑	SPL↑
1	Probabilistic	5.08	62.2	54.4	48.8
2	Probabilistic	4.94	60.8	54.2	48.9
3	Probabilistic	4.91	63.2	55.5	49.6
3	DINOV2-based	6.29	56.1	44.7	39.5
4	Probabilistic	5.23	60.2	52.5	46.4

Table 6: Ablation study of the dynamic modeling on VLN-CE R2R Val-Unseen split.

Dynamic Method	NE↓	OS↑	SR↑	SPL↑
Base	5.29	61.9	52.6	47.1
w/ FDS (epoch-1)	6.13	56.0	44.6	38.7
w/ FDS (epoch-2)	5.06	60.1	51.0	45.2
w/ FDS (epoch-3)	5.06	62.4	53.9	48.2
w/ IDS	4.91	63.2	55.5	49.6

construction (Noised IDS), thereby breaking the alignment between actions and visual transitions while keeping the VLN data and training scale unchanged. This leads to a significant drop in navigation performance, as noisy supervision introduces inconsistent training signals for action tokens, which confirms that IDS primarily benefits the model by reinforcing fine-grained action-visual dynamics consistency, rather than merely increasing data size. We further reformulate IDS as a multiple-choice question (MCQ), where the model selects the correct action from four candidates instead of directly generating the action token. Although action-grounded visual dynamics is preserved, navigation performance slightly decreases. While the MCQ format allows the model to rely on simple comparison or elimination among candidate options, the generative IDS requires the agent to directly produce the action token based solely on the visual change. Sharing the same generative action space with VLN decoding is therefore important, as it ensures that the transition knowledge learned during IDS can be directly applied to action prediction during navigation, leading to more robust behavior. We also implement a privileged distillation (PD) variant. A teacher model is first trained with IDS supervision, and its knowledge is then distilled into a student on the VLN task by minimizing the KL divergence between their action distributions. Despite this additional supervision, PD performs similarly to the baseline without dynamic supervision and remains inferior to NAVIDA. We attribute this limited improvement to how the understanding of action-grounded visual dynamics is transferred. PD enforces alignment only at the output distribution level, encouraging the student to imitate the teacher’s final predictions. Such post-hoc supervision treats visual dynamics knowledge as a fixed action signal injected after training. In contrast, NAVIDA jointly optimizes IDS and VLN within a unified framework, allowing action-visual alignment to be continuously learned and reinforced through shared representations. This tighter coupling enables action-grounded visual dynamics to directly shape navigation reasoning, yielding more effective learning than distillation-based approaches.

Correlation Between IDS and Navigation Performance. To quantify the consistency between the IDS-inferred and ground-truth action sequences, we define an **IDS score** based on the discrepancy of their resulting simulator states. Rolling out the predicted sequence $\hat{\mathbf{a}}$ and the ground-truth sequence \mathbf{a} yields final poses $(\hat{\mathbf{p}}, \hat{\theta})$ and (\mathbf{p}, θ) , where $\mathbf{p} \in \mathbb{R}^3$ denotes position and θ the yaw angle. The

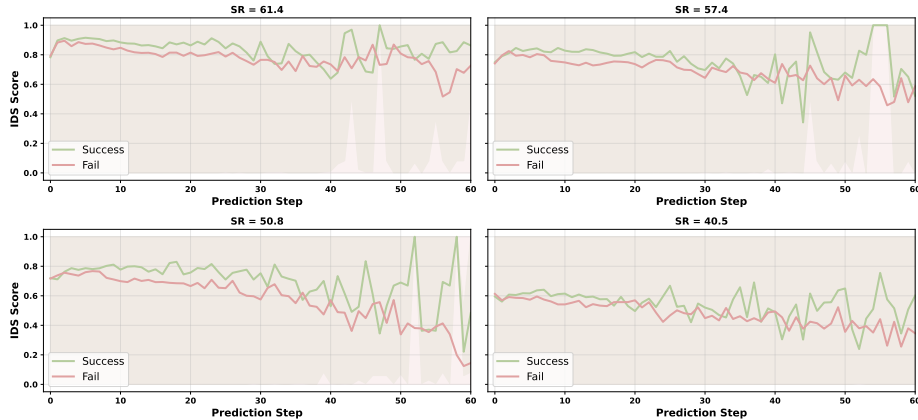


Fig. 5: IDS score over prediction steps for successful and failed trajectories. Successful episodes exhibit consistently higher and more stable IDS scores, while failed episodes show gradual degradation, indicating the importance of accurate action-state alignment for long-horizon navigation.

positional and angular discrepancy is computed as:

$$\Delta_p = \|\hat{\mathbf{p}} - \mathbf{p}\|_2, \quad \Delta_\theta = \min\left(\left|\hat{\theta} - \theta\right|, 2\pi - \left|\hat{\theta} - \theta\right|\right). \quad (3)$$

The IDS score is then defined as:

$$\text{IDS}_{\text{Score}} = \exp\left(-\frac{\Delta_p}{\sigma_p}\right) \cdot \exp\left(-\frac{\Delta_\theta}{\sigma_\theta}\right), \quad (4)$$

where σ_p and σ_θ control the sensitivity to positional and angular deviations, respectively. In our implementation, we set $\sigma_p = 0.1$ and $\sigma_\theta = \pi/12$.

Fig. 5 shows the evolution of IDS scores over prediction steps for successful and failed trajectories under different overall success rates. Several consistent trends can be observed. At early stages, the IDS scores of successful and failed episodes are similar, indicating that short-term action prediction is generally reliable in both cases. As navigation proceeds, however, the two curves gradually diverge: successful trajectories maintain higher and more stable IDS scores, whereas failed ones exhibit a steady decline. This widening gap suggests that the understanding and accurate prediction of action-induced visual transitions becomes increasingly important for long-horizon navigation. Furthermore, settings with higher overall success rates consistently present higher and more stable IDS scores. This strong association indicates that IDS accuracy reflects the model’s capability to understand the visual dynamics of its actions. When this understanding is precise, action sequences remain coherent over time, leading to improved navigation performance. In contrast, lower IDS scores in failed trajectories imply weaker understanding of the action–visual dynamics, where small deviations accumulate and ultimately result in failure.

Ablations of HPAC. Tab. 5 presents an ablation study of HPAC on the VLN-CE R2R val-unseen split. We first analyze the effect of the maximum number of action chunks. When the maximum is set to 1 with merging probability fixed to 1, HPAC reduces to the deterministic action-merging strategy adopted in prior work [7, 44]. The best performance is achieved when allowing up to 3 action chunks under our default probabilistic merging scheme, while using fewer or more chunks degrades results. This suggests that moderately extended chunks enhance longer-horizon planning, whereas overly long chunks may exceed the model’s effective perception range and lead to suboptimal decisions. Importantly, the probabilistic merging strategy introduces controlled randomness into chunk boundaries, preserving diversity of action chunks and improving robustness to minor execution fluctuations. We also evaluate a deterministic alternative based on DINOv2 [24] similarity, where adjacent frames are grouped according to visual similarity. This variant performs worst overall. We attribute this to the fact that DINOv2 primarily captures high-level semantic similarity, whereas navigation depends on geometric and viewpoint changes. For instance, observing the same object from different viewpoints may yield high DINOv2 similarity despite significant spatial displacement. Such semantically driven and deterministic merging can obscure motion cues and reduce segmentation diversity, resulting in weaker action supervision and inferior performance.

Inverse vs. Forward Dynamics. To evaluate the effectiveness of inverse dynamics supervision, we compare it with forward dynamics supervision (FDS), as both aim to enhance action-grounded visual dynamics modeling. Following MonoDream [33], FDS predicts future visual features using the same VLM without introducing additional modules. Considering its slower convergence, we train FDS for three epochs to assess both effectiveness and efficiency relative to IDS. As shown in Tab. 6, IDS consistently outperforms both FDS and the baseline without dynamic supervision, while FDS initially causes noticeable performance degradation. We attribute this gap to differences in output space alignment and optimization difficulty. Predicting dense future visual features requires modeling high-dimensional appearance variations, which is challenging for a pre-trained VLM and typically demands more training (e.g., MonoDream trains for five epochs). In contrast, IDS shares the same output space as action prediction in VLN, making it better aligned with the model’s pre-training and downstream objectives. Although FDS gradually improves with additional training and eventually surpasses the baseline after three epochs, it still lags behind IDS, which achieves superior performance after only one epoch. These results indicate that IDS provides more stable and data-efficient supervision, whereas FDS requires longer optimization to learn reliable future-state predictions.

5 Conclusion

In this work, we presented NAVIDA, a unified VLN framework that integrates policy learning with action-grounded visual dynamics modeling. Through chunk-based inverse-dynamics supervision, NAVIDA achieves more interpretable and

stable navigation. The proposed hierarchical probabilistic action chunking mechanism structures navigation trajectories into multi-level motion units, providing richer and longer-range supervision for inverse dynamics learning. Extensive experiments demonstrate that NAVIDA achieves superior navigation performance with fewer parameters compared to state-of-the-art methods, and real-world robot evaluations confirm its effectiveness and practical applicability.

A Prompts for Different Tasks

We use task-specific prompts for VLN and for inverse-dynamics supervision, both expressed in the same action grammar (action-type + numeric tokens).

For vision-language navigation task, we use the following prompt template to instruct the model to predict the corresponding action chunks:

Imagine you are a robot programmed for navigation tasks. You have been given a video of historical observations: <image>,...,<image>and current observation: <image>. Your assigned task is: [Instruction]. Analyze this series of images to decide your next move, which could involve turning left or right by a specific degree, moving forward a certain distance.

Among them, [Instruction] is the language instruction given for the current navigation task. For inverse-dynamics supervision, we use prompt a prompt template like the following:

Imagine you are a robot programmed for navigation tasks. You have been given an image of current view <image>and an image of the goal view <image>. Analyze the two images to predict the navigation action that would move the robot from the current viewpoint to the goal view, which could involve turning left or right by a specific degree or moving forward a certain distance.

For the multiple-choice question (MCQ) of IDS, the prompt is like follows:

Imagine you are a robot programmed for navigation tasks. You have been given an image of current view <image>and an image of the goal view <image>. Analyze the two images to predict the navigation action that would move the robot from the current viewpoint to the goal view. Select the correct answer from the four options (A, B, C, or D). Options: \n A. <action A>\n B. <action B>\n C. <action C>\n D. <action D>

For the forward-dynamics supervision, the requirement is to predict the visual observation features of the next time step based on the given historical frames and language instructions. We use the following prompt:

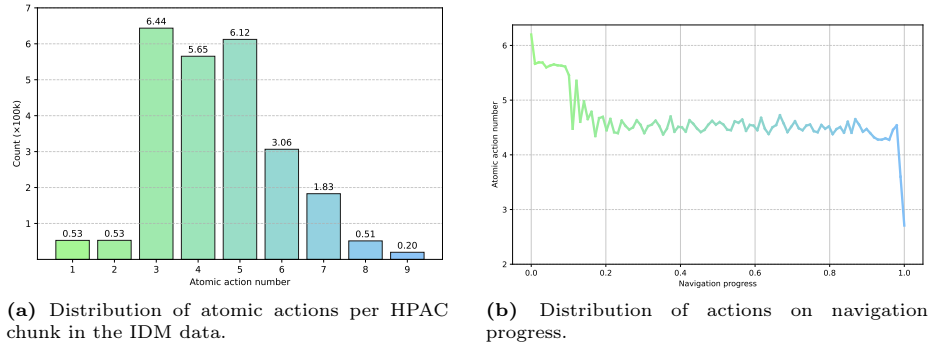


Fig. 6: Atomic action statistics of HPAC in the dataset.

Imagine you are a robot programmed for navigation tasks. You have been given a video of historical observations: $\langle \text{image} \rangle, \dots, \langle \text{image} \rangle$ and current observation: $\langle \text{image} \rangle$. Your assigned task is: [Instruction]. Analyze this series of images to predict the future observation.

B More Implementation Details

B.1 Data Details

Fig. 6a depicts the distribution of atomic actions per HPAC chunk in our inverse-dynamics (IDM) dataset. Although most chunks contain 3 to 5 atomic actions, which consistent with the fixed chunk sizes used in prior works [7, 37, 44], a non-negligible portion of samples contain either fewer or more atomic actions. Longer chunks encode larger egocentric viewpoint shifts and parallax, yielding strong, informative supervision signals for inverse dynamics and supporting long-horizon planning by offering the model an extended temporal context. In contrast, shorter chunks emphasize subtle, fine-grained visual changes (e.g., small turns or local re-alignments), which facilitate precise control and reduce action ambiguity at short horizons. This natural mixture of long and short chunks serves as a complementary curriculum: HPAC contributes global structural cues for planning alongside local adjustment priors for stabilization, thereby improving the model’s understanding of action-grounded visual dynamics and actions and improving robustness to compounding errors during execution.

We also normalized the navigation process to a range of 0 to 1, and Fig. 6b shows the distribution of action chunks as the navigation process progresses. It can be seen that in the early stages of navigation, HPAC merges a large number of atomic actions, which decreases slightly and stabilizes in the middle stages. In the later stages of navigation, closer to the target, HPAC tends to use fewer atomic actions to stabilize the robot’s position.

B.2 Training Hyperparameters

NAVIDA is implemented on Qwen-2.5-VL-3B; the vision encoder is frozen and only the projector and LLM are trainable. We use AdamW with lr = $2e-5$, BF16, Flash-Attention v2, global batch size = 64; additional hyperparameters are summarized in Tab. 7.

Table 7: Training hyperparameters used for fine-tuning Qwen2.5-VL. Only the projector and LLM modules are trainable.

Hyperparameter	Value
Training epochs	1
Trainable modules	Projector + LLM
Learning rate	$2e-5$
Optimizer	AdamW
AdamW β_1	0.9
AdamW β_2	0.999
Adam ϵ	$1e-8$
Lr schedule	Linear
Global batch size	64
Gradient accumulation	4
Mixed precision type	BFloat16
Attention type	Flash Attention v2
LLM sequence length	64800
Image resolution	308×252

B.3 Evaluation Metrics Details

To formalize the evaluation criteria and relate each metric to its practical intuition, we report Navigation Error (NE), Success Rate (SR), Oracle Success Rate (OSR), Success-weighted Path Length (SPL), and normalized Dynamic Time Warping (nDTW). In brief, lower is better for NE; higher is better for SR/OSR/SPL/nDTW.

Navigation Error (NE). NE measures the final distance between the agent’s stopping position \mathbf{p}_T and the goal location \mathbf{g} . It is defined as:

$$\text{NE} = d(\mathbf{p}_T, \mathbf{g}), \quad (5)$$

where $d(\cdot, \cdot)$ denotes the geodesic distance in the navigation environment. Smaller NE indicates better terminal accuracy.

Success Rate (SR). A navigation episode is considered successful if the agent stops within a threshold distance τ from the goal. The success rate is defined as:

$$\text{SR} = \frac{1}{N} \sum_{i=1}^N \mathbf{1}[d(\mathbf{p}_T^{(i)}, \mathbf{g}^{(i)}) \leq \tau], \quad (6)$$

where N is the total number of episodes and τ is set to 3 in most VLN settings. Higher SR reflects more consistent goal completion.

Oracle Success Rate (OSR). OSR evaluates whether the agent was ever within the success radius τ during its entire trajectory, regardless of its final stop:

$$\text{OSR} = \frac{1}{N} \sum_{i=1}^N \mathbf{1} \left[\min_t d(\mathbf{p}_t^{(i)}, \mathbf{g}^{(i)}) \leq \tau \right]. \quad (7)$$

where $\mathbf{p}_t^{(i)}$ is the t -th position of the robot in the i -th episode. OSR is informative for understanding recoverability and premature stopping.

Success-weighted Path Length (SPL). SPL measures the efficiency of successful navigation, comparing the shortest geodesic path length $L^{(i)}$ with the agent’s actual traversed path length $P^{(i)}$:

$$\text{SPL} = \frac{1}{N} \sum_{i=1}^N \mathbf{1} [d(\mathbf{p}_T^{(i)}, \mathbf{g}^{(i)}) \leq \tau] \cdot \frac{L^{(i)}}{\max(P^{(i)}, L^{(i)})}. \quad (8)$$

SPL is 0 for failures (via the indicator) and approaches 1 when successful paths are near-optimal.

Normalized Dynamic Time Warping (nDTW). nDTW measures the trajectory similarity between the agent path $\{\mathbf{p}_t\}_{t=1}^T$ and the shortest-path reference trajectory $\{\mathbf{q}_k\}_{k=1}^K$ using dynamic time warping distance $\text{DTW}(\cdot, \cdot)$:

$$\text{nDTW} = \exp \left(- \frac{\text{DTW}(\mathbf{p}_{1:T}, \mathbf{q}_{1:K})}{\eta} \right), \quad (9)$$

where η is a normalization constant (typically the shortest-path length). This exponential normalization converts the alignment cost into a bounded similarity score within the range $(0, 1]$, where values closer to 1 indicate higher spatial and temporal consistency with the optimal reference trajectory. Intuitively, nDTW rewards trajectories that closely follow the correct route, even if their timing or step correspondence differs slightly. Compared to simple geometric distance metrics, nDTW provides a more flexible and robust measure of path-following quality, as it accounts for local temporal misalignments and route overlaps that commonly occur during navigation.

B.4 Real-World Deployment Details

Fig. 7a shows the overall architecture of our real-world deployment system. Specifically, NAVIDA was deployed on a remote computation server equipped with an NVIDIA RTX 4090 GPU. The system follows a client-server structure, where the robot functions as the client that collects sensory data and executes movement commands, while the remote server is responsible for high-level reasoning and action prediction.

During operation, the robot continuously captures RGB images from its front-facing camera (as shown in Fig. 7b) and receives natural language or

voice commands from the user through a local area network. The sensory data and corresponding commands are then packaged and transmitted to the remote server via the internet. On the server side, the NAVIDA model processes these inputs, performs vision-language reasoning, and predicts the next navigation action. The predicted motion command is then sent back to the robot, where it is converted into executable parameters such as linear velocity, angular velocity, and movement duration through the robot’s motion control API.

In addition, we provide demonstration videos of real-world deployment, which are submitted together with the supplementary materials. The slight latency observed in the videos mainly results from **network communication delays** between the robot and the remote server.

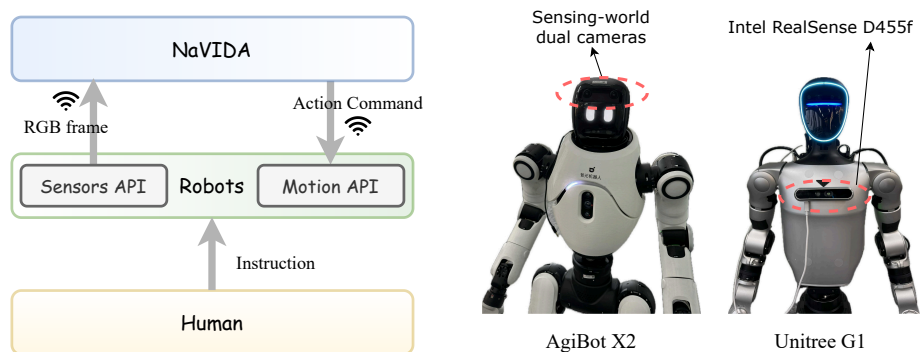


Fig. 7: Real-world evaluation setup.

Table 8: Ablation study of the vision encoder fine-Tuning on VLN-CE R2R Val-Unseen split.

Vision Encoder	NE↓	OS↑	SR↑	SPL↑
Trainable	5.12	63.6	55.6	49.2
Frozen	4.91	63.2	55.5	49.6

C More Experiment Results

C.1 More Ablations

Data Scale. Fig. 8 illustrates the performance trend of NAVIDA on R2R-CE Val-Unseen as a function of the total data size, which includes both IDS and VLN data. We also constructed a validation set for an IDS on R2R-CE Val-Unseen and plotted the variation curve of the IDS score. As the total data size increases, NAVIDA consistently achieves better performance. The improvement is particularly pronounced when the data scale is small, indicating that NAVIDA effectively leverages additional data to learn more robust representations in low-data regimes. However, as the total data scale continues to grow, the performance gains gradually saturate. This behavior likely reflects a diminishing returns effect, where the model has already captured most of the useful patterns from the available data, and further increases in data size contribute less to performance. Additionally, the stabilization may indicate that other factors such as model capacity, task complexity, or inherent noise in the data become the limiting factors once a certain data threshold is reached.

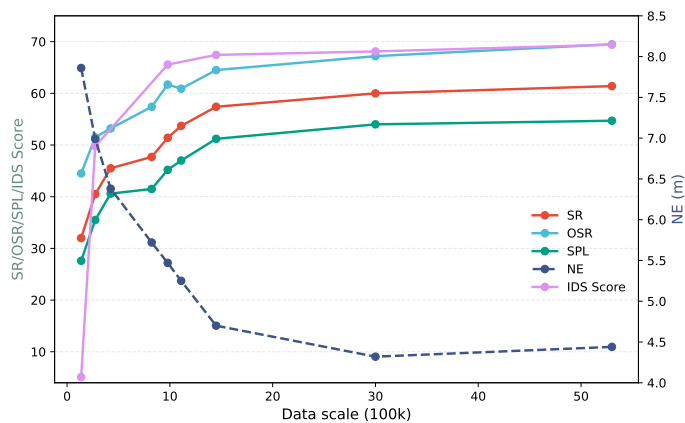


Fig. 8: Navigation performance of NAVIDA on VLN-CE R2R Val-Unseen split with the increase of data scale. SR/OSR/SPL/IDS Score increase and NE decreases as data grows, with gains tapering at larger scales.

Vision Encoder: Frozen vs. Trainable. We conduct an ablation study to evaluate the impact of fine-tuning the vision encoder on overall navigation performance. As shown in Tab. 8, unfreezing the vision encoder and training it end-to-end provides only marginal improvements compared to keeping it frozen. This result suggests that the pre-trained visual representations are already sufficiently informative for downstream navigation tasks, and further adaptation offers limited benefit. Moreover, fine-tuning substantially increases GPU memory usage and training time, with minimal returns in accuracy. Therefore, we

keep the vision encoder frozen in all subsequent experiments, enabling the model to efficiently utilize robust pre-trained visual features while maintaining a favorable balance between performance and computational efficiency.

Number of History Frames. We perform an ablation study to investigate how the number of historical frames influences navigation performance on the R2R-CE Val-Unseen split. All models are trained solely on the R2R training data for consistency. As shown in Tab. 9, using 8 history frames is sufficient to capture most instruction horizons, providing the model with adequate temporal context for action reasoning. Increasing the number of frames to 16 does not yield noticeable performance gains and occasionally leads to a slight degradation, likely due to redundant or noisy visual information accumulated over longer sequences. This behavior aligns with findings from NaVILA [7], indicating that excessive historical context can dilute the relevance of recent observations and hinder temporal grounding. Hence, we adopt 8 history frames as a balanced choice between contextual richness and model efficiency.

Table 9: Ablation study of the number of history frames on VLN-CE R2R Val-Unseen split.

# History Frames	NE↓	OS↑	SR↑	SPL↑
8	6.99	51.5	40.5	35.5
16	7.02	50.1	40.4	36.1

C.2 More Qualitative Results

We present extensive qualitative results of NAVIDA in both real-world and simulated environments to further demonstrate its effectiveness and generalization ability, as shown in Fig. 9, Fig. 10, and Fig. 11. The results show that NAVIDA produces smooth, instruction-aligned trajectories in simulation and robustly executes navigation commands in real-world settings. These findings highlight the model’s strong cross-domain generalization, accurate language grounding, and reliable decision-making in complex, long-horizon navigation tasks.

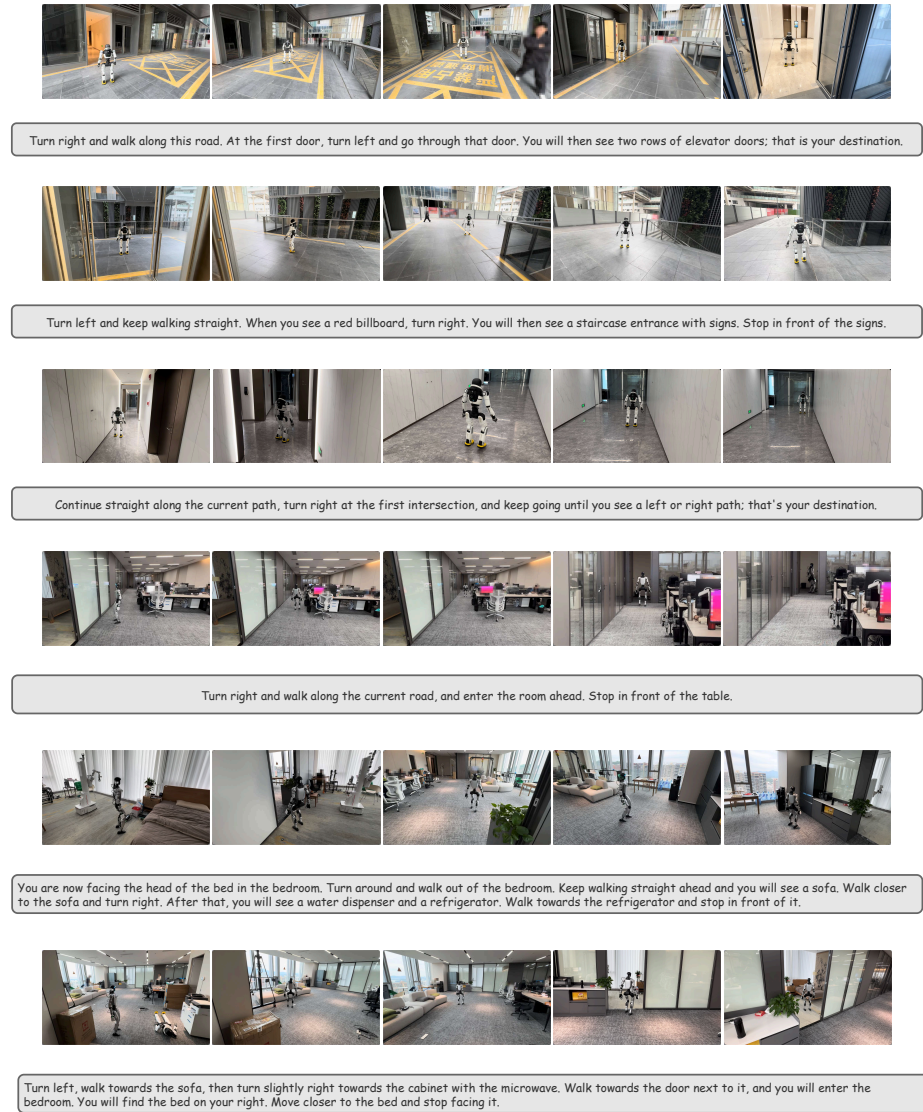


Fig. 9: Qualitative results of NAVIDA on real world.



Fig. 10: Qualitative results of NAVIDA on VLN-CE R2R Val-Unseen split.

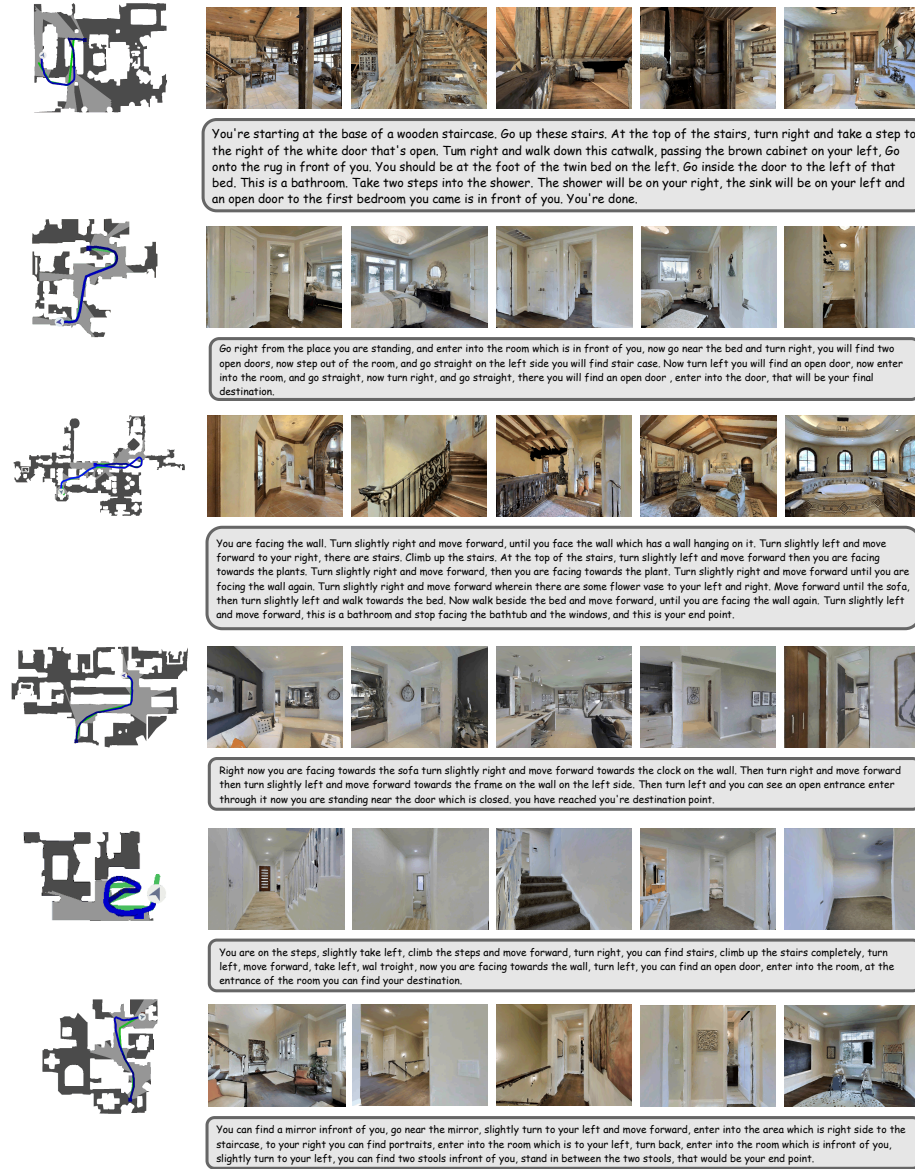


Fig. 11: Qualitative results of NAVIDA on VLN-CE RxR Val-Unseen split.

References

1. An, D., Qi, Y., Li, Y., Huang, Y., Wang, L., Tan, T., Shao, J.: Bevbort: Multimodal map pre-training for language-guided navigation. arXiv preprint arXiv:2212.04385 (2022)
2. An, D., Wang, H., Wang, W., Wang, Z., Huang, Y., He, K., Wang, L.: Etpnav: Evolving topological planning for vision-language navigation in continuous environments. *IEEE Transactions on Pattern Analysis and Machine Intelligence* (2024)
3. Anderson, P., Wu, Q., Teney, D., Bruce, J., Johnson, M., Sünderhauf, N., Reid, I., Gould, S., Van Den Hengel, A.: Vision-and-language navigation: Interpreting visually-grounded navigation instructions in real environments. In: *Proceedings of the IEEE conference on computer vision and pattern recognition*. pp. 3674–3683 (2018)
4. Bai, S., Chen, K., Liu, X., Wang, J., Ge, W., Song, S., Dang, K., Wang, P., Wang, S., Tang, J., et al.: Qwen2. 5-vl technical report. arXiv preprint arXiv:2502.13923 (2025)
5. Cai, W., Peng, J., Yang, Y., Zhang, Y., Wei, M., Wang, H., Chen, Y., Wang, T., Pang, J.: Navdp: Learning sim-to-real navigation diffusion policy with privileged information guidance. arXiv preprint arXiv:2505.08712 (2025)
6. Chen, S., Guhur, P.L., Schmid, C., Laptev, I.: History aware multimodal transformer for vision-and-language navigation. *Advances in neural information processing systems* **34**, 5834–5847 (2021)
7. Cheng, A.C., Ji, Y., Yang, Z., Zou, X., Kautz, J., Biyik, E., Yin, H., Liu, S., Wang, X.: Navila: Legged robot vision-language-action model for navigation. *Robotics: Science and Systems* (2025)
8. Chi, C., Xu, Z., Feng, S., Cousineau, E., Du, Y., Burchfiel, B., Tedrake, R., Song, S.: Diffusion policy: Visuomotor policy learning via action diffusion. *The International Journal of Robotics Research* **44**(10-11), 1684–1704 (2025)
9. Contributors, I.: InternNav: InternRobotics’ open platform for building generalized navigation foundation models. <https://github.com/InternRobotics/InternNav> (2025)
10. Dou, Z.Y., Gao, F., Peng, N.: Masked path modeling for vision-and-language navigation. arXiv preprint arXiv:2305.14268 (2023)
11. Georgakis, G., Schmeckpeper, K., Wanchoo, K., Dan, S., Mitsakaki, E., Roth, D., Daniilidis, K.: Cross-modal map learning for vision and language navigation. In: *Proceedings of the IEEE/CVF conference on computer vision and pattern recognition*. pp. 15460–15470 (2022)
12. Hong, Y., Wang, Z., Wu, Q., Gould, S.: Bridging the gap between learning in discrete and continuous environments for vision-and-language navigation. In: *Proceedings of the IEEE/CVF conference on computer vision and pattern recognition*. pp. 15439–15449 (2022)
13. Hong, Y., Wu, Q., Qi, Y., Rodriguez-Opazo, C., Gould, S.: Vln bert: A recurrent vision-and-language bert for navigation. In: *Proceedings of the IEEE/CVF conference on Computer Vision and Pattern Recognition*. pp. 1643–1653 (2021)
14. Huang, Y., Wu, M., Li, R., Tu, Z.: Vista: Generative visual imagination for vision-and-language navigation. arXiv preprint arXiv:2505.07868 (2025)
15. Krantz, J., Gokaslan, A., Batra, D., Lee, S., Maksymets, O.: Waypoint models for instruction-guided navigation in continuous environments. In: *Proceedings of the IEEE/CVF International Conference on Computer Vision*. pp. 15162–15171 (2021)

16. Krantz, J., Lee, S.: Sim-2-sim transfer for vision-and-language navigation in continuous environments. In: European conference on computer vision. pp. 588–603. Springer (2022)
17. Krantz, J., Wijmans, E., Majumdar, A., Batra, D., Lee, S.: Beyond the nav-graph: Vision-and-language navigation in continuous environments. In: European Conference on Computer Vision. pp. 104–120. Springer (2020)
18. Ku, A., Anderson, P., Patel, R., Ie, E., Baldrige, J.: Room-across-room: Multilingual vision-and-language navigation with dense spatiotemporal grounding. arXiv preprint arXiv:2010.07954 (2020)
19. Li, J., Bansal, M.: Improving vision-and-language navigation by generating future-view image semantics. In: Proceedings of the IEEE/CVF conference on computer vision and pattern recognition. pp. 10803–10812 (2023)
20. Liu, R., Wang, X., Wang, W., Yang, Y.: Bird’s-eye-view scene graph for vision-language navigation. In: Proceedings of the IEEE/CVF International Conference on Computer Vision. pp. 10968–10980 (2023)
21. Liu, Z., Zhu, L., Shi, B., Zhang, Z., Lou, Y., Yang, S., Xi, H., Cao, S., Gu, Y., Li, D., et al.: Nvila: Efficient frontier visual language models. In: Proceedings of the Computer Vision and Pattern Recognition Conference. pp. 4122–4134 (2025)
22. Long, Y., Cai, W., Wang, H., Zhan, G., Dong, H.: Instructnav: Zero-shot system for generic instruction navigation in unexplored environment. arXiv preprint arXiv:2406.04882 (2024)
23. Nguyen, K., Dey, D., Brockett, C., Dolan, B.: Vision-based navigation with language-based assistance via imitation learning with indirect intervention. In: Proceedings of the IEEE/CVF Conference on Computer Vision and Pattern Recognition. pp. 12527–12537 (2019)
24. Oquab, M., Darcet, T., Moutakanni, T., Vo, H., Szafraniec, M., Khalidov, V., Fernandez, P., Haziza, D., Massa, F., El-Nouby, A., et al.: Dinov2: Learning robust visual features without supervision. arXiv preprint arXiv:2304.07193 (2023)
25. Raychaudhuri, S., Wani, S., Patel, S., Jain, U., Chang, A.X.: Language-aligned waypoint (law) supervision for vision-and-language navigation in continuous environments. arXiv preprint arXiv:2109.15207 (2021)
26. Ross, S., Gordon, G., Bagnell, D.: A reduction of imitation learning and structured prediction to no-regret online learning. In: Proceedings of the fourteenth international conference on artificial intelligence and statistics. pp. 627–635. JMLR Workshop and Conference Proceedings (2011)
27. Savva, M., Kadian, A., Maksymets, O., Zhao, Y., Wijmans, E., Jain, B., Straub, J., Liu, J., Koltun, V., Malik, J., et al.: Habitat: A platform for embodied ai research. In: Proceedings of the IEEE/CVF international conference on computer vision. pp. 9339–9347 (2019)
28. Schumann, R., Zhu, W., Feng, W., Fu, T.J., Riezler, S., Wang, W.Y.: Velma: Verbalization embodiment of llm agents for vision and language navigation in street view. In: Proceedings of the AAAI Conference on Artificial Intelligence. vol. 38, pp. 18924–18933 (2024)
29. Wang, H., Liang, W., Gool, L.V., Wang, W.: Towards versatile embodied navigation. *Advances in neural information processing systems* **35**, 36858–36874 (2022)
30. Wang, H., Liang, W., Van Gool, L., Wang, W.: Dreamwalker: Mental planning for continuous vision-language navigation. In: Proceedings of the IEEE/CVF international conference on computer vision. pp. 10873–10883 (2023)
31. Wang, L., Xia, X., Zhao, H., Wang, H., Wang, T., Chen, Y., Liu, C., Chen, Q., Pang, J.: Rethinking the embodied gap in vision-and-language navigation: A holis-

- tic study of physical and visual disparities. In: Proceedings of the IEEE/CVF International Conference on Computer Vision. pp. 9455–9465 (2025)
32. Wang, S., Wang, Y., Li, W., Cai, X., Wang, Y., Chen, M., Wang, K., Su, Z., Li, D., Fan, Z.: Aux-think: Exploring reasoning strategies for data-efficient vision-language navigation. arXiv preprint arXiv:2505.11886 (2025)
 33. Wang, S., Wang, Y., Li, W., Wang, Y., Chen, M., Wang, K., Su, Z., Cai, X., Jin, Y., Li, D., et al.: Monodream: Monocular vision-language navigation with panoramic dreaming. arXiv preprint arXiv:2508.02549 (2025)
 34. Wang, Z., Li, X., Yang, J., Liu, Y., Jiang, S.: Gridmm: Grid memory map for vision-and-language navigation. In: Proceedings of the IEEE/CVF International conference on computer vision. pp. 15625–15636 (2023)
 35. Wang, Z., Li, X., Yang, J., Liu, Y., Jiang, S.: Sim-to-real transfer via 3d feature fields for vision-and-language navigation. arXiv preprint arXiv:2406.09798 (2024)
 36. Wang, Z., Li, J., Hong, Y., Wang, Y., Wu, Q., Bansal, M., Gould, S., Tan, H., Qiao, Y.: Scaling data generation in vision-and-language navigation. In: Proceedings of the IEEE/CVF international conference on computer vision. pp. 12009–12020 (2023)
 37. Wei, M., Wan, C., Yu, X., Wang, T., Yang, Y., Mao, X., Zhu, C., Cai, W., Wang, H., Chen, Y., et al.: Streamvln: Streaming vision-and-language navigation via slowfast context modeling. arXiv preprint arXiv:2507.05240 (2025)
 38. Wu, Q., Gong, X., Xu, K., Manocha, D., Dong, J., Wang, J.: Towards target-driven visual navigation in indoor scenes via generative imitation learning. *IEEE Robotics and Automation Letters* **6**(1), 175–182 (2020)
 39. Wu, S., Fu, X., Wu, F., Zha, Z.J.: Vision-and-language navigation via latent semantic alignment learning. *IEEE Transactions on Multimedia* **26**, 8406–8418 (2024)
 40. Yao, X., Gao, J., Xu, C.: Navmorph: A self-evolving world model for vision-and-language navigation in continuous environments. arXiv preprint arXiv:2506.23468 (2025)
 41. Zeng, S., Qi, D., Chang, X., Xiong, F., Xie, S., Wu, X., Liang, S., Xu, M., Wei, X.: Janusvln: Decoupling semantics and spatiality with dual implicit memory for vision-language navigation. arXiv preprint arXiv:2509.22548 (2025)
 42. Zhang, J., Li, A., Qi, Y., Li, M., Liu, J., Wang, S., Liu, H., Zhou, G., Wu, Y., Li, X., et al.: Embodied navigation foundation model. arXiv preprint arXiv:2509.12129 (2025)
 43. Zhang, J., Wang, K., Wang, S., Li, M., Liu, H., Wei, S., Wang, Z., Zhang, Z., Wang, H.: Uni-navid: A video-based vision-language-action model for unifying embodied navigation tasks. *Robotics: Science and Systems* (2025)
 44. Zhang, J., Wang, K., Xu, R., Zhou, G., Hong, Y., Fang, X., Wu, Q., Zhang, Z., Wang, H.: Navid: Video-based vlm plans the next step for vision-and-language navigation. *Robotics: Science and Systems* (2024)
 45. Zhang, P., Su, Y., Wu, P., An, D., Zhang, L., Wang, Z., Wang, D., Ding, Y., Zhao, B., Li, X.: Cross from left to right brain: Adaptive text dreamer for vision-and-language navigation. arXiv preprint arXiv:2505.20897 (2025)
 46. Zhang, Y., Wu, J., Li, W., Li, B., Ma, Z., Liu, Z., Li, C.: Video instruction tuning with synthetic data. arXiv preprint arXiv:2410.02713 (2024)
 47. Zhang, Z., Zhu, W., Pan, H., Wang, X., Xu, R., Sun, X., Zheng, F.: Activevln: Towards active exploration via multi-turn rl in vision-and-language navigation. arXiv preprint arXiv:2509.12618 (2025)